Available online at www.sciencedirect.com
ScienceDirect
Earth and Planetary Science Letters 255 (2007) 485–493
EPSL
www.elsevier.com/locate/epsl

Grain growth kinetics of $CaIrO_3$ perovskite and post-perovskite, with implications for rheology of D″ layer

Takashi Yoshino *, Daisuke Yamazaki

Institute for Study of the Earth's Interior, Okayama University, Tottori 682-0193, Japan

Received 11 October 2006; received in revised form 27 November 2006; accepted 7 January 2007
Available online 13 January 2007
Editor: G.D. Price

Abstract

Grain growth kinetics of $CaIrO_3$ perovskite and post-perovskite aggregates was investigated by time-series experiments at pressures of 2 and 3 GPa and temperatures ranging from 1373 to 1773 K in a piston cylinder apparatus. The experiments were conducted in the stability field of both perovskite and post-perovskite. The increase of grain size (G) with time (t) follows a growth law: $G^n - G_0^n = k \cdot t$ ($k = k_0 \exp(-H^*/RT)$). The growth exponents (n) for perovskite and post-perovskite are 2.6 ± 0.5 and 4.5 ± 0.9, respectively. The activation enthalpy (H^*) of post-perovskite grain growth is 251 ± 35 kJ/mol. Grain growth of post-perovskite is distinctly slower than that of perovskite. Sluggish grain growth of the post-perovskite is caused by its strong anisotropic shape. The phase transition from the perovskite to the post-perovskite at the D" discontinuity would lead to maintenance of small grain size in the D" layer. If diffusion creep is the dominant deformation mechanism of post-perovskite, the phase transformation would induce the significant softening of the D" layer due to slow growth rate of post-perovskite compared with a situation without the phase transition.

Keywords: diffusion creep; D″ layer; grain growth; provskite; post-perovskite; rheology

1. Introduction

Large seismic anomalies have been observed at the bottom of lower mantle with a thickness of several hundreds kilometers (D″ layer) [e.g., 1,2]. The anomalies of the D″ layer are difficult to explain with known physical properties of $MgSiO_3$ perovskite—the main constituent of the lower mantle. The recent discovery of the $MgSiO_3$ post-perovskite phase transition has provided new insights into the D″ layer from high-pressure experiments with the diamond anvil cell (DAC) [3,4]. The transition pressure of $MgSiO_3$ perovskite to post-perovskite (125 GPa) is consistent with the depth of the velocity increase at the D″ seismic discontinuity (2700 km depth) [2]. In order to understand the dynamics near the core–mantle boundary, it is, therefore, important to clarify the physical properties of the post-perovskite phase. Rheology is one of the important properties that control dynamic processes. To assess the dynamics of descending slabs to the core–mantle boundary and upwelling of the materials from the D″ layer, it is essential to understand the rheological behavior of post-perovskite.

For polycrystalline aggregates, the grain size of constituent materials is a key parameter to determine the dominant deformation mechanism because the transition between dislocation and diffusion creep during plastic deformation is controlled by grain size. In

* Corresponding author. Tel.: +81 858 43 3734; fax: +81 858 43 3450.
E-mail address: tyoshino@misasa.okayama-u.ac.jp (T. Yoshino).

0012-821X/$ - see front matter © 2007 Elsevier B.V. All rights reserved.
doi:10.1016/j.epsl.2007.01.010

addition, the viscosity of the diffusion creep regime is a function of the grain size of the constituent materials. Therefore, several experimental studies of the grain growth kinetics for mantle minerals have been conducted to understand rheology of the mantle [5–8].

The $MgSiO_3$ post-perovskite structure is unquenchable to ambient conditions. The phase is only stable over 100 GPa [3], which can be attained only by DAC experiment. Long duration heating experiment needed to observe kinetic processes is quite difficult in the DAC. A useful analog is $CaIrO_3$ because it has the same structure as the $MgSiO_3$ post-perovskite phase (space group: *Cmcm*) at atomospheric pressure. Hirose and Fujita [9] demonstrated that there is a phase transition of $CaIrO_3$ from post-perovskite (called post-perovskite hereafter) to a perovskite-type structure (space group: *Pbnm*), which is isostructural with $MgSiO_3$ perovskite, with increasing temperature under pressure. Therefore, $CaIrO_3$ can be considered as a good analog for both $MgSiO_3$ perovskite and post-perovskite and can be used to examine physical properties of both perovskite and post-perovskite structures. To this end in this study we investigated the growth kinetics of $CaIrO_3$ post-perovskite and perovskite. These data were used to further an understanding of the rheological behavior across the phase boundary from perovskite to post-perovskite near the bottom of lower mantle.

2. Experimental procedure

The starting material for grain growth experiment of post-perovskite was synthetic $CaIrO_3$ post-perovskite prepared from a mixture of reagent-grade IrO_2 and $CaCO_3$. At room pressure, the mixture was heated in air for over 24 h at 1073 K to remove carbon dioxide. At this stage, the mixture was composed of $CaIr_2O_4$ and IrO_2 with a small amount of $CaIrO_3$ post-perovskite seed. The retrieved sample was finely ground in agate mortar and then heated in air for 240 h at 1253 K. At 1 atm, 1253 K is in their stability field of post-perovskite [10]. The recovered sample was a single-phase $CaIrO_3$ post-perovskite from X-ray power diffraction. Starting powder for grain growth of perovskite was synthesized from the $CaIrO_3$ post-perovskite powder at 1 GPa and 1723 K for 30 min using 3/4″-diameter furnace assembly in a piston cylinder apparatus. The perovskite phase was confirmed by X-ray power diffraction.

We conducted two series of annealing experiments to determine the grain growth rates of $CaIrO_3$ perovskite and post-perovskite using 1/2″-diameter furnace assembly in a piston cylinder apparatus. The experimental cell assemblies were composed of talc outermost sleeves and Pyrex glass sleeves enclosing a graphite heater. The vertical spacers were made of MgO. The starting material was placed in a Pt capsule with 2.0 mm outer diameter surrounded by MgO. The temperature was controlled with a $W_{95}Re_5$–$W_{74}Re_{26}$ thermocouple. Pressure was applied at room temperature. The sample was then heated at a constant ramp rate of 200 °C per minute to the desired temperature. Quenching to room temperature was achieved within a minute. Pressure was then released to atmospheric pressure.

Table 1
Experimental conditions and results

Run no.	*P* (GPa)	*T* (K)	*t* (h)	*G* (μm)
Post-perovskite				
PPVGG38*	3	1373	0	2.0
PPVGG31	3	1373	48	12.7
PPVGG33	3	1373	192	18.8
PPVGG23	3	1473	48	14.0
PPVGG29	3	1473	192	23.7
PPVGG32	3	1573	12	15.8
PPVGG27	3	1573	48	21.2
PPVGG24	3	1673	3	16.5
PPVGG25	3	1673	12	24.5
PPVGG26	3	1673	48	29.3
Perovskite				
PPVGG39*	2	1773	0	41.0
PPVGG35	2	1773	1	47.4
PPVGG37	2	1773	4	66.6
PPVGG36	2	1773	16	99.8

G denotes the mean diameter of $CaIrO_3$ crystals obtained from intercept method [13,14].
*, the zero time run was terminated when the temperature reached the prescribed value by shutting off the heating power supply.

A series of the grain growth experiments with post-perovskite were conducted at a range of temperatures from 1373 to 1673 K at 3 GPa. Because the stability field of perovskite is very narrow [9], a series of the grain growth experiments for perovskite were conducted at a fixed temperature of 1773 K at 2 GPa. To determine the initial grain sizes (G_0), zero time experiments were conducted at 1373 K and 1773 K for post-perovskite and perovskite, respectively.

After an experiment, the samples were mounted in epoxy resin and initially polished with a diamond powder. Final polishing was done with colloidal silica. Phase identification and microstructural observation were carried out with a micro-beam X-ray diffractometer in reflection geometry and a scanning electron microscope. Grain sizes were measured at a magnification of ×20–100 (dependent on the grain size) using a reflecting optical microscope except for the experiment PPVGG38. Because the grain size of the zero time

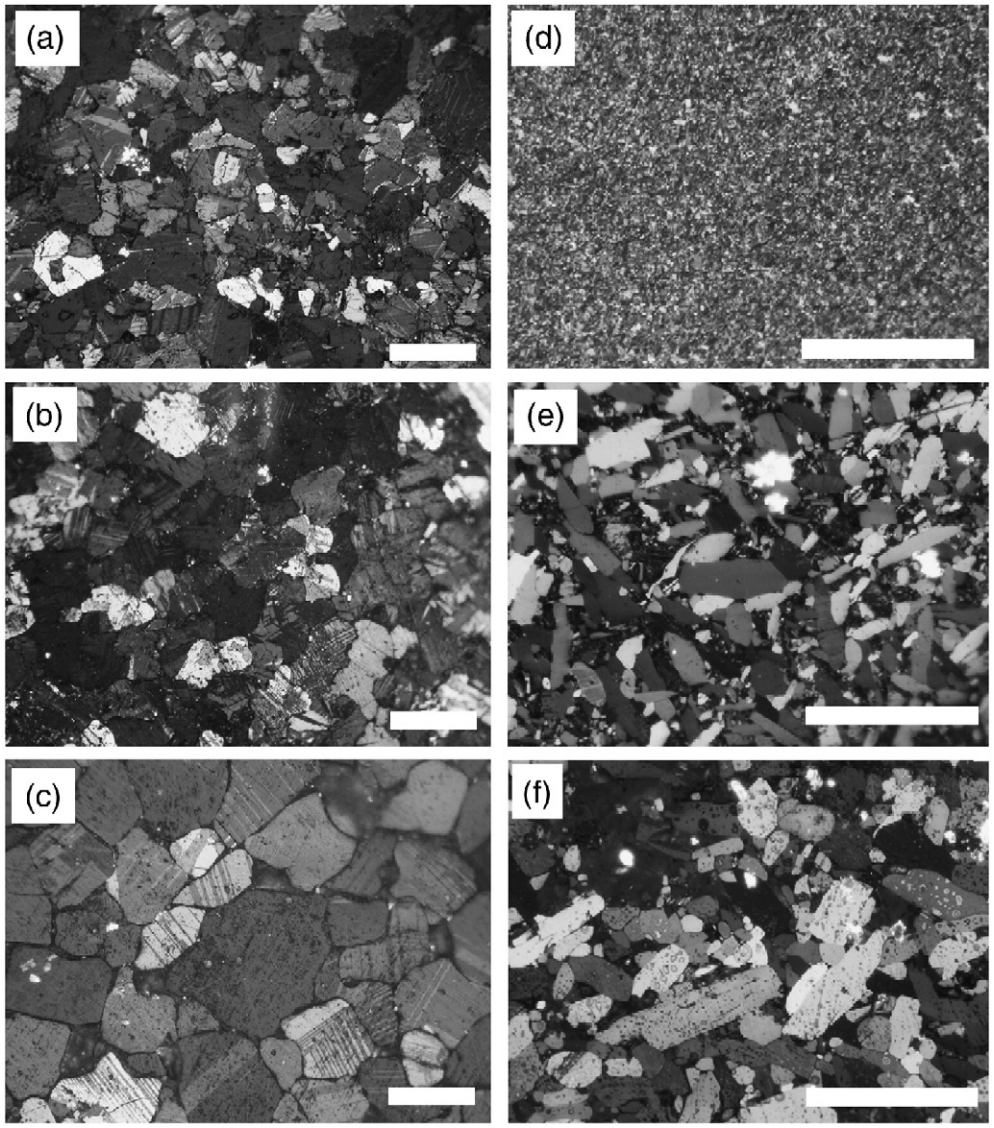

Fig. 1. Reflection optical images showing run products of $CaIrO_3$ perovskite and post-perovskite in polished section. (a) Perovskite Run# PPVGG39 (0 h and 1773 K). (b) Perovskite Run# PPVGG37 (4 h and 1773 K). (c) Perovskite Run# PPVGG36 (16 h and 1773 K). (d) Post-perovskite Run# PPVGG38 (0 h and 1373 K). (e) Post-perovskite Run# PPVGG24 (3 h and 1673 K). (f) Post-perovskite Run# PPVGG26 (48 h and 1673 K). White scale bars indicate 100 μm.

experiment of post-perovskite (PPVGG38) was quite small, the initial grain size was determined with a scanning electron microscope.

The 3-dimensional (3D) grain size distribution was evaluated by variations of the intercept length along analyzed lines and the grain area on the polished section. These distributions are possible to be different from the 3D grain size distribution by sectioning effect. Therefore, we investigated the sectioning effect for each one sample of perovskite and post-perovskite. The variation of intercept length was determined from the measurement of the length between two intercepts (i.e., grain boundary) along the analyzed lines. The 2-dimensional (2D) grain size distributions were made by image analysis. The grain boundaries were traced on screen from the digitized images. Image analysis was conducted for each binary image by using Image J software for Macintosh provided by NIH. The Schwarz–Saltykov method [11] based on the probability of polished sections resulting from the intercept of spheres was used to estimate the 3D grain size distribution from the determined 2D distribution.

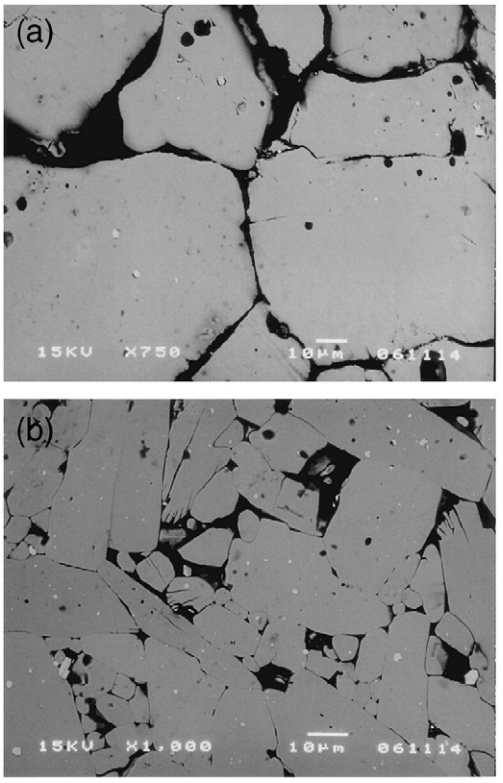

Fig. 2. Back-scattered electron images of (a) perovskite (Run# PPVGG36) and (b) post-perovskite aggregate (Run# PPVGG25) showing occurrence of impurity phase. Bright, gray and dark portions indicate IrO_2 crystals, $CaIrO_3$ crystals, and grain boundaries or plucking part, respectively. Note that small IrO_2 crystals mainly occur as an inclusion in $CaIrO_3$ crystals, and that the grain size of both phase is much larger than inter-particle distance of IrO_2.

Average grain size (G) was estimated from the measured average intercept length (L) using a relation $G=cL$, where c is a constant value of 1.56 [12]. We applied a volume-based, grid and line-sampled intercept stereographic technique to measure the intercept length of the individual grain [13,14]. On the polished section, most of the grain boundaries were opened during decompression and some grains were plucked during polishing. Therefore, we did not measure these areas. The analyzed area is composed of 200–500 grains. Experimental details and results are summarized in Table 1.

3. Results

Fig. 1 shows the reflection images of the microstructure of perovskite (Fig. 1a–c) and post-perovskite (Fig. 1d–f). This is clear evidence for grain growth of both phases. The perovskite crystals are equigranular, whereas those of post-perovskite are characterized by anisotropic shape with high aspect ratio. The grain boundaries of the post-perovskite aggregate generally are flat surface (faceting). These surfaces correspond to crystallographically controlled faces with lower interfacial energy than that produced by the curved interfaces. The orientations of minimum interfacial energy per unit area are crystallographic planes of low Miller indices [15]. Because the grains of post-perovskite are anisotropic shape but randomly oriented, the average grain size determined by the intercept method is available [13]. Although a secondary phase was not identified by X-ray diffraction, the back-scattered electron images of all the run products show a presence of tiny IrO_2 grains (<0.1 vol.%), which mainly appear as inclusion in both $CaIrO_3$ perovskite and post-perovskite (Fig. 2). We

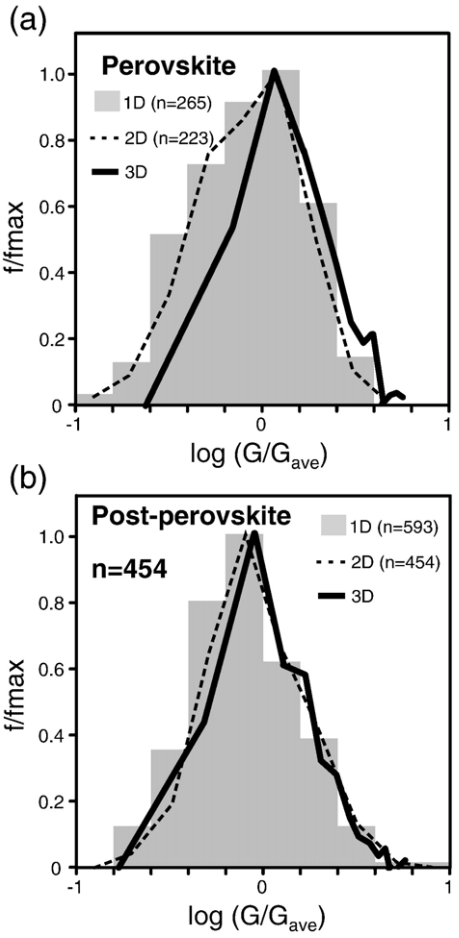

Fig. 3. Log normalized size distribution of (a) perovskite (Run# PPVGG36) and (b) post-perovskite (Run# PPVGG27). Grain size and frequency are normalized to average grain size and maximum frequency, respectively. Histograms, dashed lines and solid lines represent intercept length (1D), 2D and 3D normalized grain size distributions, respectively. The 3D grain size distributions were calculated from the 2D grain size distributions using the Schwarz–Saltykov method.

rarely observed IrO_2 grains along grain boundaries or at grain corners.

Fig. 3 shows a sectioning effect on the grain size distribution. Although the size distributions become sharp and a peak skews to larger grain size with increasing dimension (from 1D to 3D), there is no significant change for shape characteristics of the grain size distribution. The distribution of the intercept lengths in the present study seems to represent a feature of the 3D grain size distribution. We, therefore, used the distribution of the intercept lengths as the grain size distribution of the analyzed system in the following discussion.

The grain size distribution of both perovskite and post-perovskite shows a constant shape (Fig. 4) when the size distribution is normalized to the average grain size. Because uniform size distribution is independent of annealing times, it suggests that normal grain growth occurred in these systems. In addition, the maximum and minimum grain sizes were within a factor of two to three times the mean grain size, suggesting a near normal grain growth [16]. The grain size distribution for post-perovskite is nearly log normal, whereas that of perovskite is similar to the Lifshitz–Slyozov–Wagner (LSW) distribution with a peak skewed toward larger grain sizes [17,18].

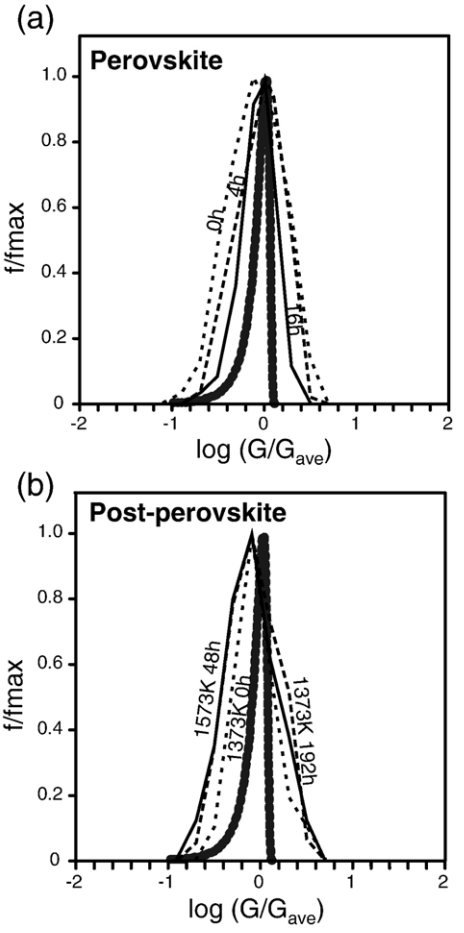

Fig. 4. Representative log grain size distributions of perovskite (a) and post-perovskite (b). The size distributions are derived from the distribution of the intercept length along the analyzed lines. Grain size and frequency are normalized to average grain size and maximum frequency, respectively. Thick dotted lines indicate interface-controlled LSW distribution [17,18].

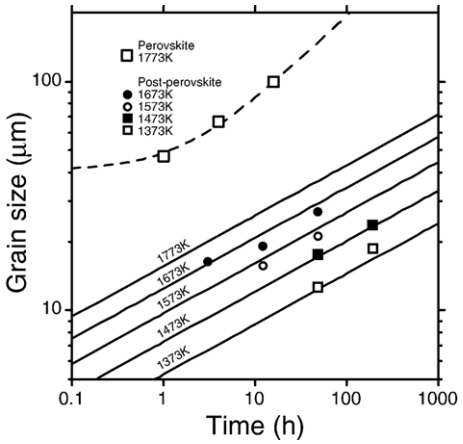

Fig. 5. Grain size variations in two-dimensional section of $CaIrO_3$ perovskite (a) and post-perovskite (b) as a function of run duration at various temperatures. Dashed and solid lines indicate the non-linear least square fit to the grain growth law, yielding $n=2.6\pm0.5$ and log $k=-15.25\pm2.06$ $m^{2.6\pm0.5}/s$, for perovskite at 1773 K (a), and $n=4.5\pm0.9$, $H=251\pm35$ kJ/mol and log $k_0=-17.95\pm3.56$ $m^{4.5\pm0.9}/s$ for post-perovskite (b), respectively.

The results for post-perovskite and perovskite coarsening at various temperatures and annealing times are summarized in Table 1 and Fig. 5. For post-perovskite, the average grain size increases with increasing annealing time at constant temperature. The relationship between log size and log time can be fitted using the following form for normal grain growth kinetics:

$$G^n - G_0^n = k \cdot t \quad (1)$$

in which G is the mean size at time t, G_0 is the mean size of starting material, k is the rate constant, and n is the growth exponent. The normal grain growth law of perovskite was calculated by a non-linear least square fitting to Eq. (1). The growth exponent (n) and rate constant (k) are determined to be 2.6 ± 0.5 and $10^{-15.25\pm2.06}$ $m^{2.6\pm0.5}/s$,

respectively. The value of k for different temperature can be obtained by the following relation:

$$k = k_0 \exp\left(-\frac{H^*}{RT}\right) \quad (2)$$

where k_0 is the pre-exponential constant, H^* is the activation enthalpy, R is the gas constant and T is absolute temperature. The normal grain growth law of post-perovskite (for which data were obtained at several temperatures) can be calculated by a non-linear least square fitting to the combination of Eqs. (1) and (2) to yield:

$$G^{4.5\pm0.9} - G_0^{4.5\pm0.9} = 10^{-17.95\pm3.56}\left(m^{4.5\pm0.9}/s\right) \cdot \exp\left(-\frac{251\pm35(\mathrm{kJ/mol})}{RT}\right) \cdot t \quad (3)$$

The errors were estimated from the standard deviation in the least square fitting. In this study, the G_0-value of post-perovskite is used to be 2.0 μm from the zero time experiment at 1373 K. The effect of grain coarsening during heating from 1373 K to the desired temperature on the determination of some parameters for the growth law is negligibly small because of the slow coarsening rate of post-perovskite.

4. Discussion

4.1. Growth mechanisms of perovskite and post-perovskite

Grain growth of isotropic system under static condition is a simple transformation in which grain size increases under driving forces arising from surface curvature [19,20]. The coarsening process of larger particles is related to the expense of smaller particles, and its driving force is minimization of interfacial energy [e.g., [21,22]. Boundary mobility is controlled by self-diffusion of rate-limited species across the boundary region (intrinsic regime) or by the mobility of impurity phase such as pore, solute and liquid film at the grain boundaries (extrinsic regime) [23]. For the intrinsic regime, the growth exponent is theoretically expected to be 2 in the grain growth of a single phase [19,24]. Although the growth exponent of perovskite ($n=2.6\pm0.5$) is higher than the value predicted from the ideal case, it is consistent with experimental values (average: $n=2.5\pm0.4$) for metals in which impurity level is very low [20]. The grain size distribution of perovskite is similar to the LSW-type grain size distribution arising from variations in the interface curvature (Fig. 4a) [17,18]. The main controlling factor for grain growth of perovskite is likely to be Ostwald ripening (dissolution of small grains and growth of larger grains by precipitation).

The growth exponent of post-perovskite ($n=4.5\pm0.9$) is considerably higher than that of perovskite. One possibility to explain such large values of n is Zener pinning [25,26], because we recognized a presence of tiny amounts of IrO_2 in the back-scattered electron images (Fig. 2). If the grains start with a size that is smaller than the inter-particle distance, they grow normally until there are enough particles interacting with the boundaries to pin the grains. If the data used in the calculation of the growth exponent included one measurement after Zener pinning occurred, the resulting growth exponent would be extremely high. In this case, the grain size becomes constant after Zener pinning occurred. Even if the average grain size is larger than the inter-particle distance, there is no evidence of cease of grain growth (Fig. 5). Because most of IrO_2 crystals appear as inclusion (Fig. 2), sweeping out and pinning of impurity phase would not play an important role in sluggish grain growth. Furthermore, although perovskite aggregates also include the same amount of impurity (IrO_2), the growth exponent of perovskite is significantly smaller than that of post-perovskite. Therefore, a large difference of growth exponents between them seems to be derived from the other factors.

The most remarkable microstructure difference between perovskite and post-perovskite is crystal shape. Perovskite aggregates have polygonal texture, whereas most of grain boundaries of post-perovskite aggregate were be faceted. Thus, the grain growth kinetics of post-perovskite is not controlled by a decrease of surface curvature. As degree of faceting on the crystal surface increases, the grain size distributions obtained from the grain growth in fluid- or melt-bearing system tend to change from the LSW distribution to the log normal distribution [27]. This behavior is consistent with the present results (Fig. 4). Therefore, the grain growth kinetics of post-perovskite is probably controlled by development of flat surface due to the relatively stronger anisotropic surface energy.

For crystals with strong anisotropy, some segments of the faceted grain boundaries are likely to be singular with atomically flat structures [15]. For anisotropic systems with large variation of the grain boundary energy, the growth exponent tends to become higher [28]. The grain boundary mobility of the post-perovskite could be limited in two-dimensional nucleation of boundary steps. A grain with a plane of lower surface energy with respect to the growth direction expands

only in lateral direction. The resultant velocity of flat surface motion is very slow. If the specific crystal plane shows faster growth in the lateral direction, the grain shape would be anisotropic. In some ceramic and metal-alloy systems, the size of the flat surface decreases gradually with increasing temperature until the surface step free energy become zero at the roughening transition temperature [29,30]. Although surface roughening can increase the grain growth at higher temperature [31], there was no noticeable change of the grain shape and growth rate in the $CaIrO_3$ post-perovskite aggregate in the 1373–1673 K temperature range. This observation suggests that the growth kinetics of the post-perovskite phase is not affected by surface roughening in this temperature range.

4.2. Application to rheology of the D″ Layer

The present results demonstrated that the anisotropy of crystal shape and faceting strongly control grain growth rate. Faceting at crystal interface is likely to appear when crystal surface has strong anisotropic interfacial energy. Degree of anisotropy of interfacial energy may be mainly caused by crystal structure [32]. Because the $MgSiO_3$ post-perovskite could form a platy crystal habit parallel to the (010) plane [3], the crystal shape is expected to be anisotropic as well as $CaIrO_3$ post-perovskite. Thus, the $CaIrO_3$ used in our experiments would be a good analog to understand grain growth mechanism of the $MgSiO_3$ post-perovskite in the lowermost mantle. In the following section, we will discuss rheology at the conditions of the D″ layer from our results of $CaIrO_3$ grain growth based on homologous temperature scaling.

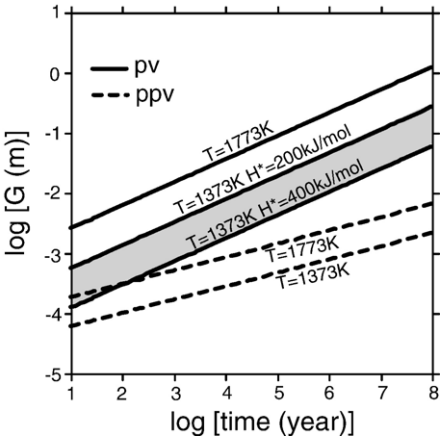

Fig. 6. Grain size evolution of $CaIrO_3$ perovskite and post-perovskite as a function of time at 1373 K ($T/T_m \sim 0.7$) and 1773 K ($T/T_m \sim 0.9$). Solid and dashed lines indicate perovskite and post-perovskite, respectively. Initial grain size (G_0) is assumed to be zero. Shaded region represents a possible range of grain size of perovskite calculated from an assumed activation enthalpy (200–400 kJ/mol) for grain growth of perovskite.

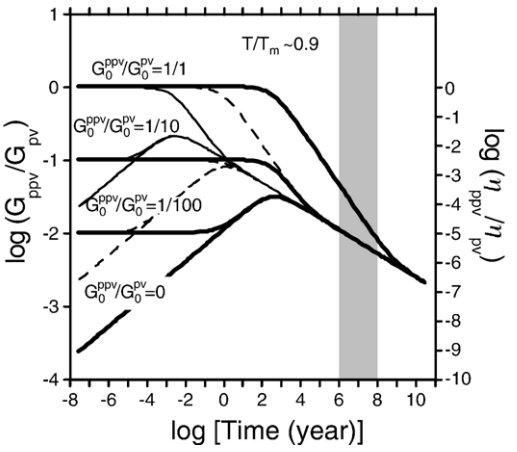

Fig. 7. Comparison of grain size and viscosity between perovskite- and post-perovskite-dominant lower mantle. The grain size ratio of $CaIrO_3$ perovskite and post-perovskite (G_{ppv}/G_{pv}) is defined as a function of time at constant temperature (1773 K: $T/T_m = \sim 0.9$). Thick solid, dashed and thin solid lines indicate the grain size and viscosity ratios when initial grain sizes of perovskite (G_0^{pv}) are 10, 1 and 0.1 mm, respectively. Initial grain sizes of post-perovskite (G_0^{ppv}) after the phase transformation from perovskite to post-perovskite were provided by a grain size ratio ($G_0^{ppv}/G_0^{pv} = 1$, 0.1, 0.01 and 0) of the two phases. Viscosities were calculated from the equation $\eta^{ppv}/\eta^{pv} \sim G^{ppv}/G^{pv}$, where η^{ppv}/η^{pv} is the relative viscosity and m is the constant of 2.5 [40]. Shaded area represents the residence time scale of the subducted slab in the D″ layer. This time scale was estimated from the velocity of plate motion and a partial length of mantle convection cell in the D″ layer.

In order to estimate the difference of grain growth between perovskite and post-perovskite, we extrapolated our experimental data in Eq. (3) to the geological time scale up to 10^8 years. Fig. 6 shows the time-dependent change of grain size at 1373 K and 1773 K, which correspond to the homologous temperature (T/T_m, where T_m is melting temperature) of ~ 0.7 and ~ 0.9, respectively [9]. The grain size of post-perovskite is much smaller than that of perovskite. Therefore, phase transformation from perovskite to post-perovskite in a descending slab would induce inhibition of grain growth. Considering that the D″ layer comprises two main phases ($MgSiO_3$ compound and ferro-periclase) and because the grain growth rate for two or more phases is much slower than that of a single phase (e.g., [6,33]), the grain growth of post-perovskite in a multi-phase assemblage is likely slower than that of a single phase. Thus, the grain size of $MgSiO_3$ post-perovskite is expected to be smaller than that in a single phase near the core–mantle boundary.

Because perovskite in the lower mantle is thought to be deformed by diffusion (grain-size sensitive) creep

[34–38], we assume that the diffusion creep is dominant deformation mechanism for post-perovskite in the D″ layer based on smaller grain size than perovskite. In diffusion creep, the viscosity of a material is expressed as a function of grain size [39,40]. From the grain growth kinetics data of both perovskite and post-perovskite, we can address effect of the perovskite to post-perovskite phase transformation on the viscosity of a descending slab in the D″ layer in the assumption that the relative viscosity (η_{ppv}/η_{pv}) is only a function of G, because the effect of the other parameters is relatively small compared to grain size controlled by a power law.

Fig. 7 shows the results of grain size and viscosity evolution at $T/T_m \sim 0.9$ with time ranging to geological time scale. First, consider the case where the grain size does not change due to the phase transition ($G_0^{ppv}/G_0^{pv} = 1$, where G_0^{pv} is the grain size of perovskite when the descending slab reaches the D″ discontinuity, and G_0^{ppv} is the grain size of post-perovskite just after the phase transformation). In the appropriate range of residence time for the slab component in the D″ layer (10^6–10^8 years), the post-perovskite viscosity decreases 3 to 6 orders of magnitude compared with the perovskite viscosity. Secondary, if significant grain size reduction occurs because of the phase transformation ($G_0^{ppv}/G_0^{pv} \ll 1$), post-perovskite grain size remains small and the resultant viscosity approaches the asymptotic line characterized by decrease of viscosity with time. In this case, the viscosity contrast between post-perovskite and perovskite reaches 5 to 6 orders of magnitude. Thus, the phase transition from the perovskite to the post-perovskite would induce the significant softening of the D″ layer because of slow growth rate of post-perovskite compared with a situation without the phase transition.

Seismic anisotropy is one of the important characteristics in the lowermost mantle [2,41–44] and is thought to be derived from the lattice preferred orientation (LPO) of constituent materials (e.g., [45–51]). However, if the dominant deformation mechanism of post-perovskite is diffusion creep, the post-perovskite aggregate would not have an anisotropic signature because these could be no LPO. The anisotropy can be interpreted by LPO of (Mg, Fe)O, which is the second abundant mineral in the lower mantle, with stronger elastic anisotropy than the post-perovskite [45,46,51,52].

Acknowledgments

We are grateful to E. Ito, T. Katsura, A. Yoneda, M. Murakami and B. Mysen for discussion and T. Matsuzaki for technical assistance. The comments of anonymous reviewer aided in improving the manuscript. This work was partially supported by a Grant-in Aid for Scientific Research No. 18740280 to TY and No. 18340173 to DY from the Japan Society for Promotion of Science and the program for the "Center of Excellence for the 21st Century in Japan".

References

[1] T. Lay, D.V. Helmberger, A lower mantle S-wave triplication and the shear velocity structure of D″, Geophys. J. R. Astron. Soc. 75 (1983) 799–838.
[2] T. Lay, Q. Williams, E.J. Garnero, The core–mantle boundary layer and deep mantle dynamics, Nature 392 (1998) 461–468.
[3] M. Murakami, K. Hirose, K. Kawamura, N. Sata, Y. Ohishi, Post-perovskite phase transition in $MgSiO_3$, Science 304 (2004) 855–858.
[4] A.R. Oganov, S. Ono, Theoretical and experimental evidence for a post-perovskite phase of $MgSiO_3$ in Earth's D″ layer, Nature 430 (2004) 445–448.
[5] S. Karato, Grain growth kinetics in olivine aggregates, Tectnophysics 168 (1989) 255–273.
[6] D. Yamazaki, T. Kato, E. Ohtani, M. Toriumi, Grain growth rates of $MgSiO_3$ perovskite and periclase under lower mantle conditions, Science 274 (1996) 2052–2054.
[7] D. Yamazaki, T. Inoue, M. Okamoto, T. Irifune, Grain growth kinetics of ringwoodite and its implication for rheology of the subducting slab, Earth Planet. Sci. Lett. 236 (2005) 871–881.
[8] Y. Nishihara, T. Shinmei, S. Karato, Grain-growth kinetics in wadsleyite: effect of chemical environment, Phys. Earth Planet. Inter. 150 (2006) 30–43.
[9] K. Hirose, Y. Fujita, Clapeyron slope of the post-perovskite phase transition in $CaIrO_3$, Geophys. Res. Lett. 32 (2005) L13313, doi:10.1029/2005GL023219.
[10] C.L. McDaniel, S.J. Schneider, Phase relations in the CaO-IrO_2-Ir system in air, J. Solid State Chem. 4 (1972) 275–280.
[11] S.A. Saltykov, The determination of the size distribution of particles in an opaque material from a measurement of the size distribution of their sections, in: H. Elias (Ed.), Stereology, Splinger, Berlin, 1967, pp. 167–173.
[12] M.I. Mendelson, Average grain size in polycrystalline ceramics, J. Am. Ceram. Soc. 52 (1969) 443–446.
[13] H.J.G. Gundersen, E.B. Jensen, Particle sizes and their distributions estimated from line- and point-sampled intercepts, Including graphical unfolding, J. Microsc. 131 (1983) 291–310.
[14] J.C. Russ, Computer Assisted Microscopy, Plenum Press, New York, NY, 1990 453 pp.
[15] D. Laporte, A. Provost, The grain-scale distribution of silicate, carbonate and metallosulfide partial melts: a review of theory and experiments, in: N. Bagdassalov, D. Laporte, A.B. Thompson (Eds.), Physics and Chemistry of Partially Molten Rocks, Kluwer Academic Publishers, Dordrecht, 2000, pp. 93–140.
[16] W.D. Kingery, H.K. Bowen, D.R. Uhlmann, Introduction to Ceramics, 2nd ed. Wiley, New York, 1976.
[17] I.M. Lifshitz, V.V. Slyozov, The kinetics of precipitation from supersaturated solid solutions, J. Phys. Chem. Solids 19 (1961) 35.
[18] C. Wagner, Theorie der altering von niederschlagen durch umlosen (Ostwald Reifung), Z. Electrochem. 65 (1961) 581.
[19] J.E. Burke, D. Turnbull, Recrystallization and grain growth, Prog. Met. Phys. 3 (1952) 220–292.

[20] H.V. Atkinson, Overview no 65: theories of normal grain growth in pure single phase systems, Acta Metall. 36 (1988) 469–492.
[21] G.W. Greenwood, Growth of dispersed precipitates in solution, Acta Metall. 4 (1956) 243–248.
[22] R.L. Joesten, Kinetics of coarsening and diffusion-controlled mineral growth, in: D.M. Kerrick (Ed.), Contact Metamorphism, Reviews in Mineralogy, vol. 26, Mineralogical Society of America, Washington, DC, 1991, pp. 507–582.
[23] M.F. Yan, R.M. Cannon, H.K. Bowen, Grain boundary migration in ceramics, in: R.M. Fulrath, J.A. Pask (Eds.), Ceramic Microstructures, Westview Press, Boulder, 1976, pp. 276–307.
[24] J.E. Burke, The Fundamentals of Recrystallization and Grain Growth, Grain Control in Industrial Metallurgy, American Society for Metals, Cleveland, Ohio, 1949, pp. 1–73.
[25] C.S. Smith, Grains, phases and interfaces an interpretation of microstructures, Trans. AIME 175 (1948) 15–51.
[26] B. Evans, J. Renner, G. Hirth, A few remarks on the kinetics of static grain growth in rocks, Int. J. Earth Sci. 90 (2001) 88–103.
[27] T. Yoshino, J.D. Price, D.A. Wark, E.B. Watson, Effect of faceting on pore geometry in texturally equilibrated rocks: implications for low permeability at low porosity, Contrib. Mineral. Petrol. 152 (2006) 169–186.
[28] A. Kazaryan, Y. Wang, S.A. Dregia, B.R. Patton, Grain growth in anisotropic system: comparison of effects of energy and mobility, Acta Mater. 50 (2002) 2491–2502.
[29] J.M. Kosterlitz, D.J. Thouless, Ordering, metastability and phase transitions in two-dimensional systems, J. Phys. C. Solid State Phys. 6 (1973) 1181–1203.
[30] H. van Beijeren, Exactly solvable model for the roughening transition of a crystal surface, Phys. Rev. Lett. 38 (1977) 993–996.
[31] Y.K. Cho, D.Y. Yoon, B.K. Kim, Surface roughening transition and coarsening of NbC grains in liquid cobalt-rich matrix, J. Am. Ceram. Soc. 87 (2004) 443–448.
[32] R. Kretz, Interpretation of the shape of mineral grains in metamorphic rocks, J. Petrol. 7 (1966) 68–94.
[33] T. Yoshino, E.B. Watson, Growth kinetics of FeS melt in partially molten peridotite: an analog for core-forming processes, Earth Planet. Sci. Lett. 235 (2005) 453–468.
[34] C. Meade, P.G. Silver, S. Kaneshima, Laboratory and seismological observations of lower mantle isotropy, Geophys. Res. Lett. 22 (1995) 1293–1296.
[35] E.J. Garnero, T. Lay, Lateral variations in lowermost mantle shear wave anisotropy beneath the north Pacific and Alaska, J. Geophys. Res. 102 (1997) 8121–8135.
[36] S. Karato, P. Li, Diffusion creep in perovskite: implications for the rheology of the lower mantle, Science 255 (1992) 1238–1240.
[37] S. Karato, S. Zhang, H.R. Wenk, Superplasticity in earth's lower mantle: evidence from seismic anisotropy and rock physics, Science 270 (1995) 458–461.
[38] P. Li, S. Karato, Z. Wang, High-temperature creep in fine-grained polycrystalline CaTiO3, an analogue material of (Mg, Fe) SiO_3 perovskite, Phys. Earth Planet. Inter. 95 (1996) 19–36.
[39] H.J. Frost, M.F. Ashby, Deformation–mechanism map, Pergamon, Oxford, 1982, pp. 16–26.
[40] R. Raj, M.F. Ashby, On grain boundary sliding and diffusional creep, Metall. Trans. 2 (1971) 1113–1127.
[41] J.-M. Kendall, P.G. Silver, Constraints from seismic anisotropy on the nature of the lower mantle, Nature 381 (1996) 409–412.
[42] M.M. Moore, E.J. Garnero, T. Lay, Q. Williams, Shear wave splitting and waveform complexity for lowermost mantle structure with low-velocity lamellae and transverse isotropy, J. Geophys. Res. 109 (2004) B02319, doi:10.1029/2003JB002546.
[43] M. Panning, B. Romanowicz, Inferences on flow at the base of Earth's mantle based on seismic anisotropy, Science 303 (2004) 351–353.
[44] E.J. Garnero, V. Maupin, T. Lay, M.J. Fouch, Variable azimuthal anisotropy in Earth's lowermost mantle, Science 306 (2004) 259–261.
[45] S. Karato, Seismic anisotropy in the deep mantle, boundary layers and geometry of mantle convection, Pure Appl. Geophys. 151 (1998) 565–587.
[46] D. Yamazaki, S. Karato, Fabric development in (Mg,Fe)O during large strain, shear deformation: implications for seismic anisotropy in earth's lower mantle, Phys. Earth Planet. Inter. 131 (2002) 251–267.
[47] T. Iitaka, K. Hirose, K. Kawamura, M. Murakami, The elasticity of the $MgSiO_3$ post-perovskite phase in the Earth's lowermost mantle, Nature 430 (2004) 442–445.
[48] N. Miyajima, K. Ohgushi, M. Ichihara, T. Yagi, Crystal morphology and dislocation microstructures of $CaIrO_3$: a TEM study of an analogue of the $MgSiO_3$ post-perovskite phase, Geophys. Res. Lett. 33 (2006) L12302, doi:10.1029/2005GL025001.
[49] A.R. Oganov, R. Martonak, A. Laio, P. Raiteri, M. Parrinello, Anisotropy of Earth's D″ layer and stacking fault in the $MgSiO_3$ post-perovskite phase, Nature 438 (2005) 1142–1144.
[50] S. Merkel, A. Kubo, L. Miyagi, S. Speziale, T.S. Duffy, H.R. Wenk, Plastic deformation of $MgGeO_3$ post-perovskite at lower mantle pressures, Science 311 (2006) 644–646.
[51] D. Yamazaki, T. Yoshino, H. Ohfuji, J. Ando, A. Yoneda, Origin of seismic anisotropy in the D″ layer inferred from shear deformation experiments on post-perovskite phase, Earth Planet. Sci. Lett. 252 (2006) 372–378.
[52] M.D. Long, X. Xiao, Z. Jiang, B. Evans, S. Karato, Lattice preferred orientation in deformed polycrystalline (Mg,Fe)O and implications for seismic anisotropy in D″, Phys. Earth Planet. Inter. 156 (2006) 75–88.